

# 1 Numerical modeling of relative contribution of planetary waves to the 2 atmospheric circulation

3 Andrey V. Koval<sup>1,2</sup>, Olga N. Toptunova<sup>2</sup>, Maxim A. Motsakov<sup>2</sup>, Ksenia A. Didenko<sup>1,2</sup>, Tatiana S.  
4 Ermakova<sup>1,2</sup>, Nikolai M. Gavrilov<sup>1</sup>, Eugene V. Rozanov<sup>3</sup>

5 <sup>1</sup>Atmospheric Physics Department, Saint-Petersburg State University, Saint Petersburg, 199034, Russia

6 <sup>2</sup>Department of Meteorological Forecasts, Russian State Hydrometeorological University, 195196 Saint-Petersburg, Russia

7 <sup>3</sup>Physikalisch-Meteorologisches Observatorium, Davos World Radiation Centre, Davos Dorf, 7260, Switzerland

8

9 *Correspondence to:* Eugene V. Rozanov (Eugene.Rozanov@pmodwrc.ch)

10 **Abstract.** Using the general circulation model of the middle and upper atmosphere (MUAM), a number of numerical scenarios  
11 were implemented to study the impact of individual planetary waves (PWs) on the global atmospheric circulation, including  
12 zonal wind, temperature, and residual meridional circulation. The calculations were performed for the winter conditions of the  
13 Northern Hemisphere (January–February). The contribution to the formation of the dynamic and temperature regimes of the  
14 middle and upper atmosphere made by equatorial Kelvin waves propagating to the east, as well as atmospheric normal modes  
15 with periods from 4 to 16 days is shown. In particular, it is demonstrated that the impact of a 5-day PW and an ultrafast Kelvin  
16 wave can change the speed of circulation flows by up to 6% in the areas of their amplitude maxima. At the same time, this  
17 effect can be significantly enhanced in certain periods of time. The presented research results are important for a deeper  
18 understanding of the mechanisms of large-scale atmospheric interactions. Despite the obviousness and simplicity of the  
19 problem, such work has not been carried out at the moment.

20 **Keywords:** planetary waves, normal atmospheric modes, residual meridional circulation, numerical simulation, atmospheric  
21 dynamics

## 22 1 Introduction

23 Planetary waves (PWs, known as Rossby waves) are large-scale variations in the hydrodynamic parameters of the  
24 atmosphere (wind, temperature, density), which are formed due to the potential vorticity conservation. The horizontal  
25 distribution of PWs is determined by the counteraction of the meridional gradient of the Coriolis force and the meridional  
26 displacements of the jet streams. According to the classic theory (e.g., Holton, 1975), a number of waves fit along the latitude  
27 circle, determining the zonal wave number. The amplitudes of PWs increase due to a decrease in the density of the atmosphere,  
28 when they propagate from their sources in the troposphere. In the middle and upper atmosphere these disturbances become an  
29 important driver of the atmospheric circulation. One of the important features of planetary waves is their active interaction

30 with the mean flow causing transfer of energy and momentum. This feature was reflected in the formulation of the generalized  
31 Eliassen Palm theorem (Eliassen and Palm, 1961). PWs can provide a significant acceleration of the background flow in the  
32 middle atmosphere when dissipating. This acceleration is comparable to the acceleration associated with gravity waves and  
33 atmospheric tides (e.g., Pogoreltsev, 1999).

34 Another important feature of PWs, which explains the need for their comprehensive study, is that they are a link  
35 between different atmospheric layers and regions. The PWs can contribute to the signal propagation from the quasi-biennial  
36 oscillation (QBO) of the equatorial zonal wind into the thermosphere (Koval et al., 2022a,b) and from the equatorial region to  
37 the extratropical region (Holton & Tan, 1980). The ability of PWs to be reflected downward at the heights of the lower  
38 thermosphere, due to changes in vertical temperature gradients associated with solar activity cycle, can also have a significant  
39 effect on the dynamic and temperature regimes of the middle atmosphere (Koval et al., 2018a).

40 According to the so-called “downward control principle” (Haynes et al., 1991), PWs are the main driving force of  
41 meridional extratropical circulation (see also Holton et al., 1995). Due to its global nature, meridional circulation is considered  
42 to be the most important mechanism of dynamic interaction between different layers and regions of the atmosphere, affecting  
43 the transport of aerosol, atmospheric gases and, consequently, the composition of the atmosphere. Changes in the meridional  
44 circulation can affect the ozone layer behavior. The state of the ozone layer has attracted increased attention due to global  
45 ozone depletion (e.g., Newman et al, 2009). PWs are the main factor in the development of sudden stratospheric warming  
46 (Schoeberl, 1978; Nath et al., 2016).

47 A lot of studies are currently dedicated to the PWs having different periods and zonal wavenumbers. For example,  
48 numerical simulations of PWs influence were discussed in Liu et al. (2004); Chang et al. (2014); Wang et al. (2017); Forbes  
49 et al. (2018; 2020); He et al. (2020) and many others. Ground based radar measurements were presented by Clark et al. (2002);  
50 Jiang et al. (2008); Pancheva et al., (2008) and satellite measurements by Day et al. (2011); Forbes & Zhang (2017); Pancheva  
51 et al., (2018); Merzlyakov et al. (2013), as well as processing of reanalysis data/weather forecasting system by Sassi et al.  
52 (2011); Qin et al. (2021), etc.

53 In this paper we considered the relative contribution of various PW modes to the formation of the global atmospheric  
54 circulation using the unique opportunity that numerical modeling gives us. In order to further understand the nature of large-  
55 scale atmospheric dynamics, we carried out a number of numerical experiments to quantify the sensitivity of the zonal wind  
56 and temperature fields, as well as meridional circulation components to the switching on/off sources of various PW modes in  
57 the model. Despite the obviousness and simplicity of the problem, such work has not been carried out at the moment.  
58 Unfortunately, there is no universal way to study the impact of all Rossby waves, each wave has its own characteristics,  
59 depending, in particular, on the season, the impact of large-scale processes such as quasi-biennial oscillation of the equatorial  
60 zonal wind, El-Nino southern oscillation, etc. Therefore, we have chosen only a part of the PW spectrum, the amplitudes of  
61 which are maximized during the boreal winter.

63 **The MUAM model.** Planetary waves are studied using the Middle and Upper Atmosphere Model (MUAM,  
64 Pogoreltsev et al., 2007). MUAM is a three-dimensional nonlinear mechanistic model of the general atmospheric circulation  
65 at heights from the surface to the F2 ionospheric layer (up to 300-400 km). This is one of the most promising and modern  
66 models of atmospheric wave dynamics, which makes it possible to study the processes in the middle and upper atmosphere, as  
67 well as their interaction with lower levels (see, for example, Gavrilov et al., 2018; Ermakova et al., 2019; Koval et al., 2018a,  
68 b; 2022a,b; Medvedeva et al., 2019). One of the advantages of MUAM is that it allows us not only to analyze the amplitudes  
69 of planetary waves, but also to associate them with various generating sources. The log-isobaric height  $x = -H \times \ln(p/p_s)$  is used  
70 as the vertical coordinate in MUAM, where  $p$  is the pressure in hPa,  $p_s$  is the surface pressure, and  $H$  is the pressure scale  
71 height. The latitude and longitude spacing of horizontal grid of the model is  $5.625^\circ \times 5^\circ$ . A version of the model with 56 vertical  
72 levels is used, covering a vertical range from the Earth surface to about 300 km. The time integration step is 225 s.

73 The MUAM radiation module takes into account atmospheric net radiative heating due to solar and infrared irradiance.  
74 The thermosphere includes parameterization of heating in the extreme ultraviolet band. Ion drag, molecular and turbulent  
75 viscosity and thermal conductivity are included as well. The model provides the possibility of planetary waves' excitation near  
76 the Earth's surface. The possibility of changing the albedo of the underlying surface is available. Weather changes and  
77 cloudiness in the troposphere are not simulated. The MUAM uses three parametrizations of gravity waves with different phase  
78 velocities, including orographic waves. For further description of the processes involved in the current version of the model,  
79 please refer to Koval et al. (2022a).

80 The main parameters simulated by the MUAM include 4-dimensional fields of the zonal, meridional and vertical  
81 velocity components, geopotential height, and temperature with time step of 2 h. By the MUAM initialization, zonal mean  
82 climatological distributions of the geopotential height and temperature are set with the lower boundary conditions at the 1000  
83 hPa isobaric level. These distributions were obtained using the reanalysis MERRA-2 data (Gelaro, et al., 2017) and averaged  
84 over 20 years (from 2000 to 2019) for January-February.

85 Since the MUAM does not reproduce tropospheric weather, the sources of the westward propagating PWs  
86 (atmospheric normal modes, NMs) and the eastward PWs (Kelvin waves) in the MUAM are specified using additional terms  
87 in the heat balance equation, having the form of time-dependent sinusoidal harmonics with zonal wavenumbers  $m = 1..3$ , and  
88 periods matching to simulated PWs. To specify the latitudinal structure of the PW components, the corresponding Hough  
89 functions obtained using the method described by Swartztrauber and Kasahara (1985) are used. PW periods are equal to the  
90 resonant response of the atmosphere to the wave action at the lower boundary (Pogoreltsev, 1999). Westward propagating  
91 NMs (1.1), (1.2), (1.3), and (2.1), (2.2) in the classification proposed by Longuet-Higgins (1968) are considered. They have  
92 periods of about 5, 10, 16 days with a zonal number of 1, and about 4 and 7 days with a zonal number of 2. In addition,  
93 eastward propagating ultrafast Kelvin wave (UFWK, having period of about 3.5 days, a zonal number of 1) are studied. In  
94 addition to the mentioned PWs, MUAM also includes sources of slow and fast Kelvin waves ( $m=1$ ), and quasi-two-day wave

95 ( $m=3$ ). However, their amplitudes and contribution to the global circulation during the boreal winter are weak, so they are  
96 beyond the scope of this study.

97 The spatial resolution of the model is relatively coarse, however, as the previous studies have shown, this resolution  
98 is more than enough to resolve global atmospheric oscillations, including tides (e.g., Suvorova & Pogoreltsev, 2011; Shevchuk  
99 et al. 2018; Didenko et al., 2021) and planetary waves (e.g., Gavrilo et al., 2018; Koval et al., 2018a,b; 2022a,b and references  
100 therein). Very important drivers of the atmospheric circulation are gravity waves (GWs). Naturally, the GWs (of orographic  
101 and non-orographic origin) cannot be resolved by the MUAM, so parameterizations are used to involve their dynamic and  
102 thermal effects. There are three of them in model. For GWs having small phase speeds (5-30 m/s) a parameterization by  
103 Lindzen (Lindzen, 1981) is implemented. For faster waves with phase speeds of 30-125 m/s, which are in particular important  
104 in the thermosphere, a version of the spectral parameterization proposed by Yigit and Medvedev (2009) is applied. The  
105 parameterization uses 15 GW spectral components uniformly distributed within the period range from 40 min to 3 h. A third  
106 parameterization implemented into the MUAM is responsible for accounting of stationary GWs of orographic origin (Gavrilo  
107 and Koval, 2013).

108 **Residual meridional circulation.** A significant problem when considering meridional flows in the framework of the  
109 classical Eulerian approach (i.e., with zonal averaging of meridional and vertical circulation flows) is that, in the equations of  
110 dynamics, the wave sources of momentum and heat are compensated by advective flows of momentum and heat (Charney and  
111 Drazin, 1961). This feature does not allow one to isolate and analyze the wave action on the mean flow. At the same time, in  
112 the continuity equation for long-lived gas components, there is a compensation of wave and mean flows. Thus, the use of the  
113 Eulerian mean meridional circulation is inefficient for calculating mass transfer and long-lived gas species and analysing wave-  
114 mean flow interaction. A thorough analysis of this topic was made by Butchart (2014). In this study, the Transformed Eulerian  
115 Mean (TEM) approach, introduced by Andrews and McIntyre (1976), was used to diagnose the impact of PW on the mean  
116 flow. The TEM approach is based on consideration of the components of the mean residual meridional circulation (RMC),  
117 which is a superposition of eddy and advective mean transport. Formulas for calculating the RMC components are presented,  
118 for example, by Koval et al. (2022a). The time-averaged RMC represents the net average movement of air masses and,  
119 therefore, in contrast to the conventional mean Eulerian circulation, it approximates of the average advective movement of  
120 atmospheric species.

121 **Scenarios of model experiments.** A series of numerical experiments (model runs) was carried out for January-  
122 February to identify the influence of various wave components on the variability of the global circulation and the RMC. The  
123 scenarios of the model runs are presented in Table 1: a reference run of the model (#1) was carried out to calculate the  
124 atmospheric circulation with the inclusion of all sources of the considered PWs, and other runs were performed with the sources  
125 of individual waves turned off. Designations of 4DW, 5DW... mean PWs having periods of 4, 5 days and others. UFKW  
126 means ultrafast Kelvin wave. The PW amplitudes were obtained using the longitude-time Fourier expansion into the first 4  
127 harmonics applied to the geopotential height fields. Next, an approximation was carried out using the least squares method to  
128 the given oscillation periods.

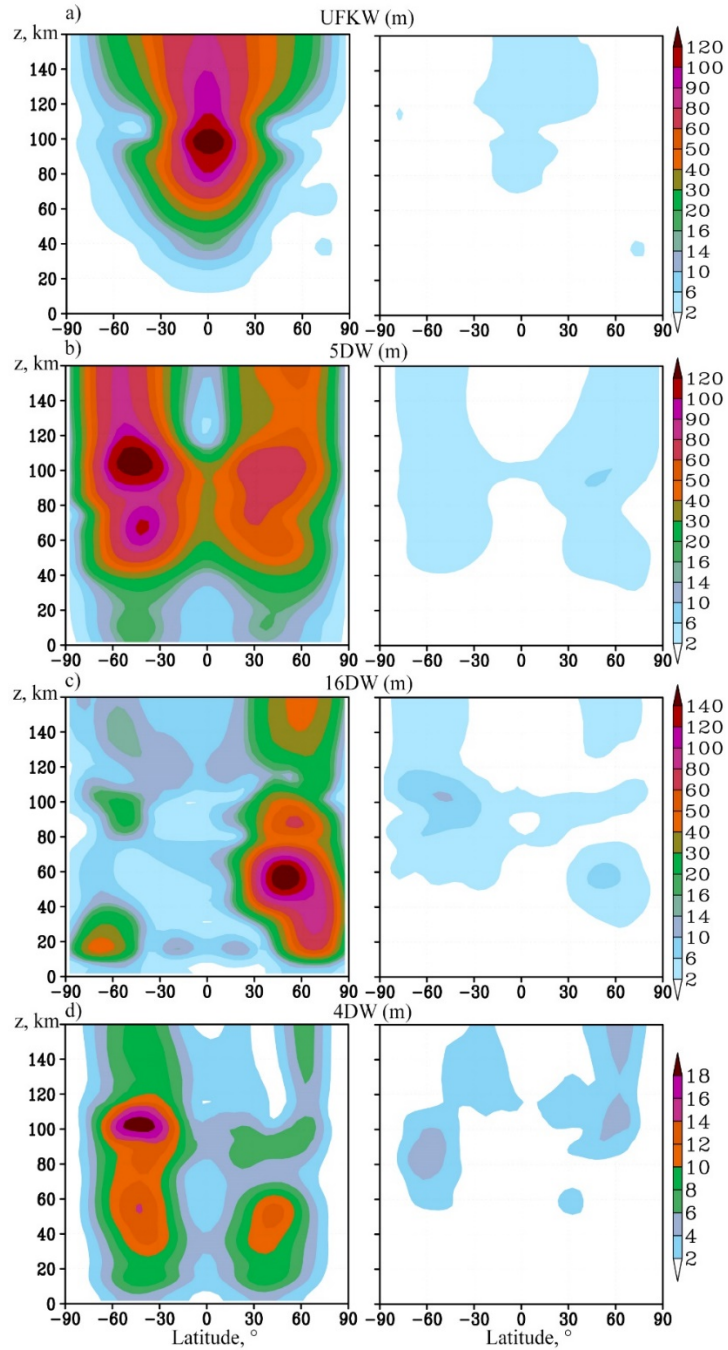
129 **Table 1. Scenarios of model calculations, including different PWs.**

runs	4DW	5DW	7DW	10DW	16DW	UFKW
1	+	+	+	+	+	+
2	+	+	+	+	+	
3	+		+	+	+	+
4	+	+	+		+	+
5	+	+	+	+		+
6		+	+	+	+	+
7	+	+		+	+	+

130

131 **3 Amplitudes of planetary waves**

132 Fig. 1 shows the amplitudes of geopotential height variations due to the observing planetary waves for January-  
 133 February. The wave amplitude according to the results of the initial model simulation with the inclusion of sources of all  
 134 considered PWs (run #1) is presented on the left side. For comparison, the right panels show the amplitudes of these waves for  
 135 the model simulations with each wave source turned off (see scenarios in Table 1).



136

137

138

139

Figure 1. Amplitudes of variations of geopotential height (m) with the source of the respective PW in the MUAM been turned on (left panels) and off (right panels) for the following PW modes: a) Ultrafast Kelvin wave, b) 5-day PW, c) 16-day (all with a zonal wave number  $m=1$ ); d) 4-day (with  $m=2$ ). Note that the color scale is different for different panels.

140 The amplitude of eastward propagating UFKW (a period of about 3.5 days) is shown in Fig. 1a. Kelvin waves are  
141 localized in the low latitude region unlike classic atmospheric NMs, the horizontal structure of which is caused primarily by  
142 the action of the Coriolis force weakening them near the equator. The UFKW is mainly excited by the tropospheric source  
143 specified in the MUAM. Its generation by internal atmospheric interactions is relatively weak (compare the left and right  
144 panels of Fig.1a). The westward propagating NMs, shown in Fig. 1b-d, have maxima in the middle latitudes of both  
145 hemispheres. Waves with larger phase velocities (4-d and 5-d NMs) can propagate in both hemispheres (Fig. 1b and 1d), while  
146 slower waves predominantly propagate through the eastward wind structures of the winter (in our case – the Northern)  
147 hemisphere (Fig.11c). This is due to propagation barriers of these waves occurring when their phase velocity is less than the  
148 westward zonal jet stream in the summer stratosphere and mesosphere (see, for example, Charney and Drazin, 1961). The  
149 presence of these barriers is also confirmed by the calculation of the refractive index of the atmosphere for the PWs considered.  
150 According to Matsuno (1970), PWs propagate along waveguides: regions of positive refractive index. Our calculations showed  
151 that in the Southern Hemisphere the waveguide for 10- and 16-day waves is interrupted, preventing their direct upward  
152 propagation. These waves propagate to the Southern Hemisphere from the Northern one, crossing the equator in the  
153 stratosphere, as was shown, for example, in the study by Koval et al. (2018a).

154 Fig. 1 shows the deficiency of waves generation in the middle atmosphere inside the model, and the PW amplitudes  
155 with the sources turned off (right panels) do not exceed a numerical noise level. An exception is the maximum amplitude of  
156 16-day PW in the right Fig. 1c, which is formed at latitude near 60° S and altitude of about 100 km. When the tropospheric  
157 source is turned off, this maximum of geopotential height reaches 15 m in the right panel of Fig. 1c, whereas it is about 24m  
158 for the turned-on wave source (the left panel of Fig.1c). This reveals an interesting effect of 16-day PW generating by internal  
159 atmospheric sources was discovered. The main source of the 16-day wave generating in the southern lower thermosphere in  
160 the MUAM may be elucidated by the nonlinear interaction of the 5- and 4-day waves, whose amplitudes have maxima in the  
161 same latitude-altitude region in the left panels of Fig. 1b and 1d. Therefore, further study of this phenomenon is required.

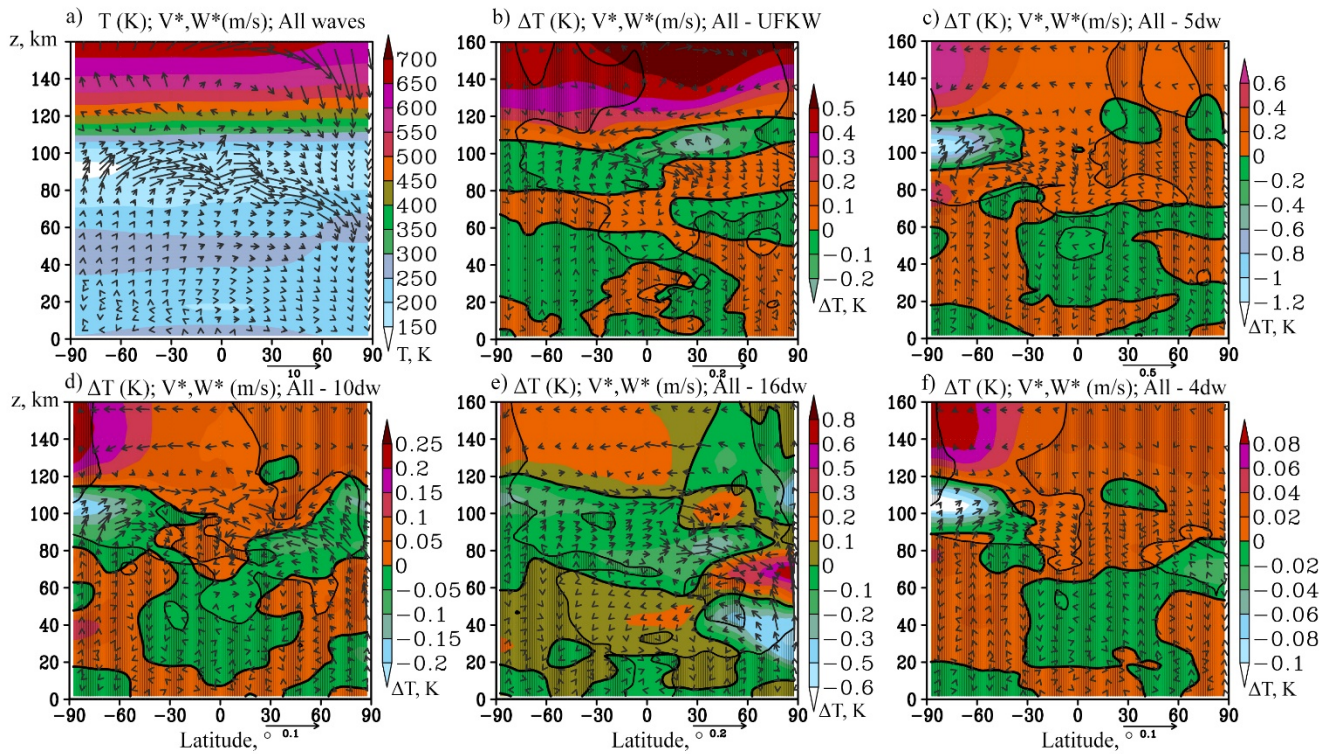
162 A detailed comparison of the MUAM-simulated PW amplitudes for January-February with satellite and radar  
163 observations, also with reanalysis data was carried out. For example, the amplitudes of PWs in the geopotential field calculated  
164 according to NCEP/NCAR reanalysis data at 10 and 30 hPa pressure levels were presented in the study by Pancheva et al.,  
165 (2008). The values of these amplitudes agree with our results. The calculated PW amplitudes in geopotential height according  
166 to the MERRA-2 reanalysis data and averaged over the years used for the initialization of MUAM have also similar value and  
167 structure to the simulated one's. Additionally, Yamazaki et al. (2021) presents the distributions of 4-day PW amplitudes  
168 according to measurements of geopotential height using Microwave Limb Sounder on Aura satellite, the structure of which  
169 corresponds to our calculations. Whereas, the presented values of the PW amplitudes may differ significantly, which is  
170 primarily due to the fact that the data for individual specific days are presented in the specified article. The data from the global  
171 numerical weather forecasting system (NOGAPS-ALPHA) is used by Sassi et al., (2012) to calculate structures of geopotential  
172 height variations by atmospheric NMs. These structures are similar to our distributions. In addition, the 5-day wave  
173 amplification in the southern mesosphere similar to the one demonstrated in the left Fig. 1a is shown. For a more detailed

174 analysis of the simulated PWs, in order to compare with the published data, the amplitudes of temperature variations by PWs  
175 were also calculated. The simulated 5-day PW and UFKW in temperature field were compared, in particular, with the wave  
176 amplitudes calculated from TIMED/SABER temperature data (Pancheva et al., 2010). The amplitude values accordance (up  
177 to 6 K at the MLT height for January for 5-day PW at the mid-latitudes of both hemispheres, for UFKW - at the equator) and  
178 the spatial distribution accordance of PW across latitudes were found. Moreover, the simulated PW amplitudes correlate in  
179 magnitude and spatial distribution with the respective waves obtained in a number of studies (Pancheva et al., 2008, 2009;  
180 Forbes et al., 2017; Pedatella & Forbes, 2009; Huang et al., 2017).

#### 181 **4 Relative PW contribution to the general atmospheric circulation**

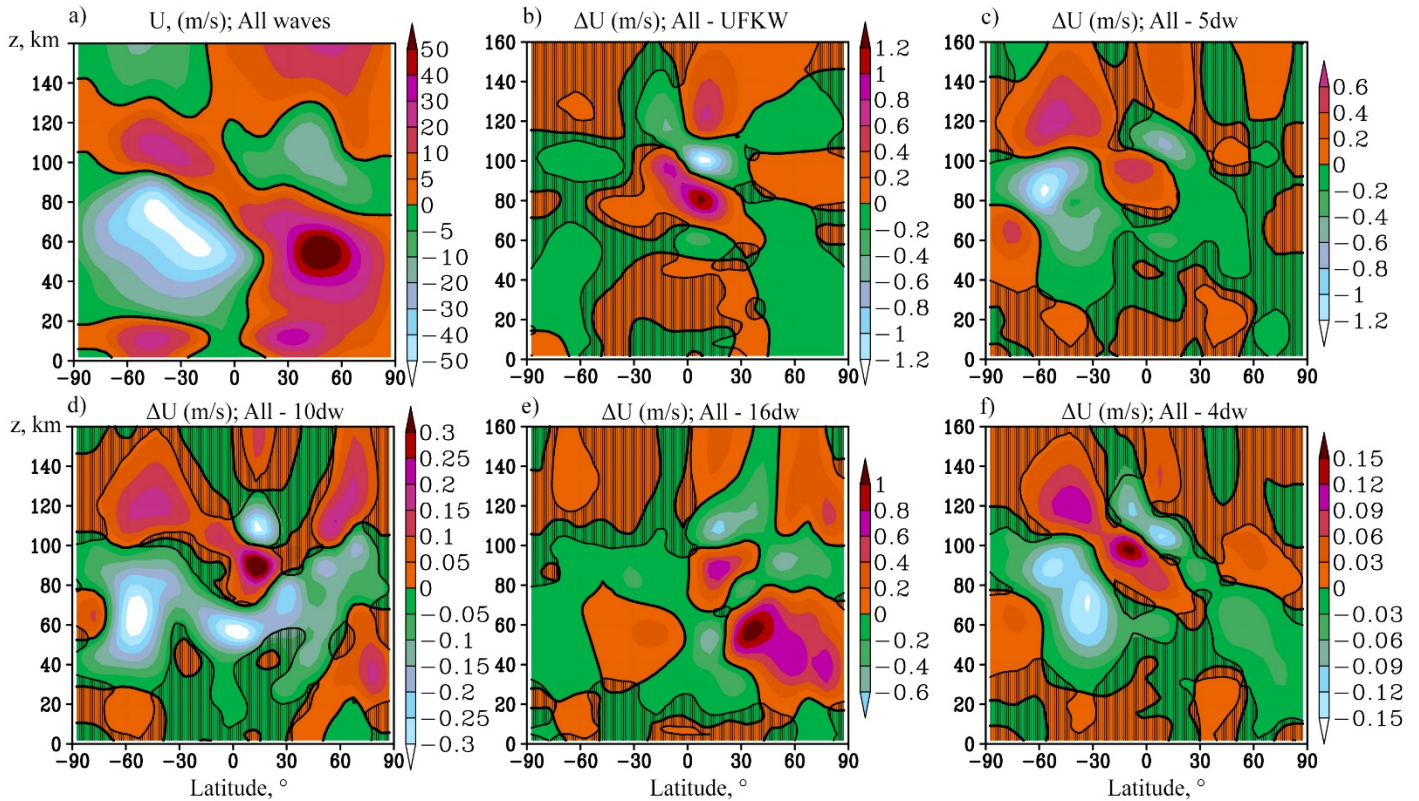
182 The residual meridional circulation (RMC) was calculated to analyze the changes in atmospheric circulation caused  
183 by various PWs for each MUAM simulation scenario presented in Table 1, with all PW sources turned on for comparisons  
184 with model runs at turned-off sources of particular wave modes. The RMC structure should be sensitive to the PW impact as  
185 it is a combination of advective and wave-induced eddy components. The latter is driven primarily to PWs according to the  
186 “Downward control principle” (Haynes et al., 1991). Fig. 2 shows the RMC components and temperature averaged over  
187 January-February for model calculation No. 1 (all PW sources included) and differences in these fields due to turning off each  
188 of analysed PW mode. Respective zonal-mean zonal wind increments are shown in Fig. 3. Simulated zonal-mean wind (Fig.  
189 3a) and temperature (Fig. 2a) correlate with those obtained with the empirical models HWM-14 (Drob et al., 2015) and  
190 NRLMSIS 2.0 (Emmert et al., 2020), also with a semiempirical wind model by Jacobi et al. (2009) and with the MERRA-2  
191 reanalysis data.





192  
193  
194  
195  
196

Figure 2. a) RMC components (arrows, m/s, vertical component multiplied by 200) and mean zonal temperature components (colours, K) for January-February with all PW sources turned on; b-f) increments in RMC and temperature due to switching off sources of PW: UFKW, 5-, 10-, 16- and 4-day waves, respectively. Shaded areas show insignificant temperature and/or RMC increments at 95%.



197  
198  
199  
200

**Figure 3. a) zonal wind components (colours, m/s) for January-February with all PW sources turned on; b-f) increments in zonal wind due to switching off sources of PW: UFKW, 5-, 10-, 16- and 4-day waves. Shaded areas show insignificant wind increments at 95%.**

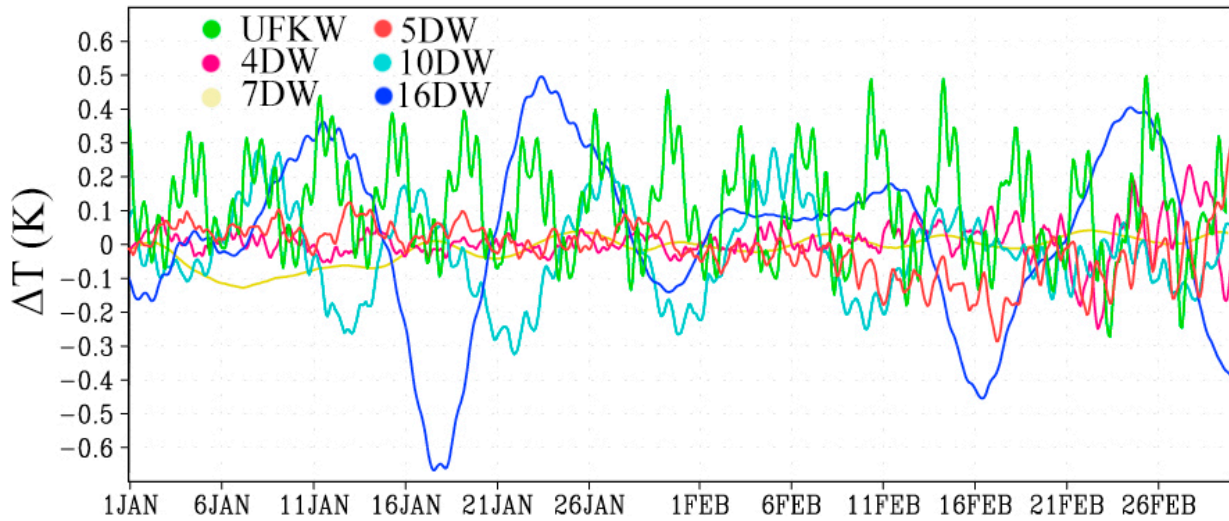
201  
202  
203  
204  
205  
206  
207  
208  
209  
210  
211  
212  
213

Fig. 2 and 3 show influence of turning off each individual PW to the zonal-mean temperature and zonal wind. The main impacts are usually localized in the regions of maximum PW amplitudes. The greatest contribution to the circulation change is made by 5-day PW. The main differences in Fig. 2c occur in the southern lower thermosphere, which correspond to a RMC strengthening in a layer between 80 and 120 km after switching on 5-d PW tropospheric source. The acceleration of zonal wind (eastward above 100 km, and westward below) is observed in the same region in Fig. 3c. This effect is primarily explained by the convergence of the Elissen-Palm flux (EP) in this region. The acceleration of the RMC there leads to the lifting up of a warmer air and warming of the atmospheric layer between 60 and 90 km, as well as to the acceleration of air transport from the coldest region of the atmosphere (about 90 km, at latitudes from the South Pole to 60° N), which leads to the cooling of the atmosphere above this layer. In addition, in the circumpolar southern stratosphere, at a level of about 60 km, there is deceleration of the zonal wind, which, on the contrary, is associated with the EP flux divergence. The described changes in RMC and zonal wind between 60 and 120 km can reach values up to 6% forming a significant contribution to the atmospheric circulation from only one wave. Relative changes in RMC components and zonal wind are presented in Figs.S1b-S3b in the supplemental information.

214 The maximum UFKW amplitude is located at 100 km in the equatorial region (see Fig. 1b). Then the wave propagates  
215 higher, gradually attenuating. Its contribution to the circulation flows changes is also maximized in this region and exerted  
216 mainly in the strengthening of the zonal wind (Fig. 3b) and the RMC (Fig. 2b). Similar to 5-day PW, the RMC increments can  
217 reach up to 5-6% as it is shown in Figs. Figs.S1a and S2a. Fig S3a shows that zonal mean wind changes in the equatorial  
218 region, between 80 and 120 km can exceed 10% in areas where wind values are greater than 5 m/s. The UFKW impact in the  
219 100-120 km layer leads to cooling in the Northern Hemisphere caused by a slowdown in meridional transport and additional  
220 updrafts causing adiabatic cooling.

221 The impact of the 16-day wave on the circulation, as shown above (Figs. 2e and 3e), is comparable in value with 5-  
222 day PW and UFKW, however in has different structure. Maximum PW amplitude occurs in the stratosphere of the Northern  
223 Hemisphere, and its contribution to atmospheric circulation is observed in this region. Figure 2e shows that introduction of 16-  
224 day wave leads to cooling of the layer below 50 km and heating of the overlying layer. The temperature changes here are  
225 explained by the change in the RMC components: in particular, the acceleration and weakening of the RMC descending branch  
226 contributes to adiabatic heating and cooling, respectively. This is accompanied by acceleration of the zonal wind (Fig. 3e),  
227 directed in this region to the east (Fig. 3a). Statistically significant changes in circulation components may reach 6% in the  
228 high-latitude stratosphere as shown in Figs. S1d and S2d. Below, in Figs. 5 and 6 it is shown that action of the 16-day PW may  
229 be stronger than 5-day PW and UFKW at certain points in time.

230 10- and 4-day PW make a smaller contribution to the dynamic and thermal regime of the atmosphere. Specifically,  
231 the structure of the 10-day wave in the middle atmosphere is similar to the structure of the 16-day one: the amplitude maximum  
232 is observed in the northern stratosphere, but due to the higher phase velocity, its waveguide in the southern middle atmosphere  
233 is wider. Propagating in the Southern Hemisphere, it contributes to the zonal wind acceleration up to heights of 140 km (Fig.  
234 3d) and to the respective temperature changes. A faster 7-day wave, like 5-day wave, is able to propagate along waveguides  
235 in both hemispheres. Generally, the 10- and 7-day PW contributions cause the same effects as the 5-day one described above,  
236 although they are much weaker in this region.



237  
238  
239

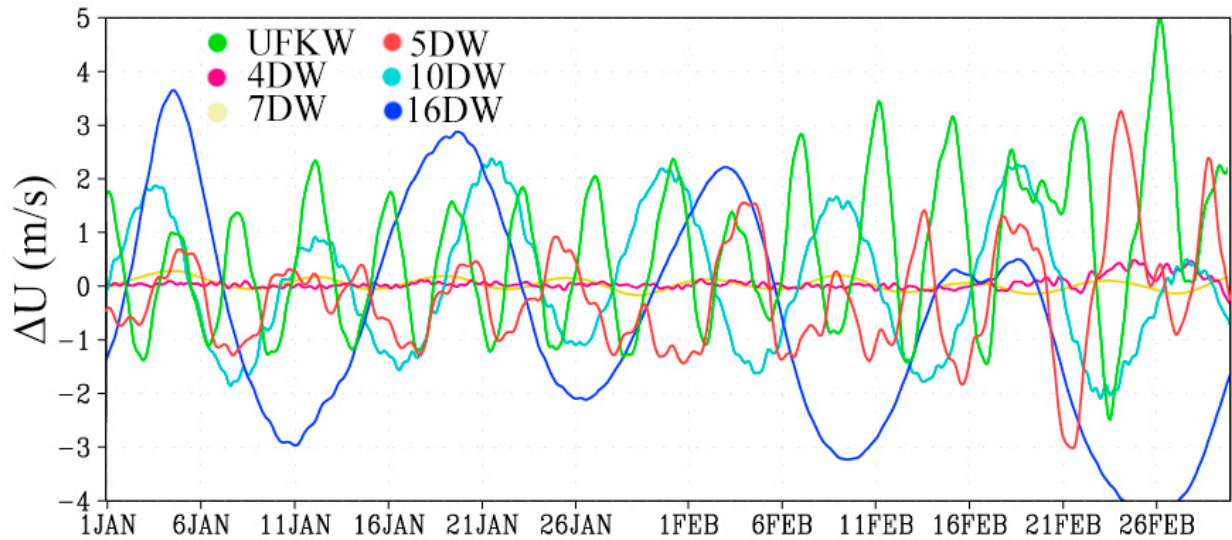
**Figure 4. Time series of mean zonal temperature variations due to the inclusion of tropospheric sources of various PW in the regions of their maximum amplitudes in the MUAM.**

240  
241  
242  
243  
244

The relatively weak increments, examined in Fig. 2 and 3, require an assessment of statistical significance. Such an assessment was carried out using the Student's paired t-test applied to 45312 pairs of samples in each of the latitude-altitude grid node (64 longitude points  $\times$  708 time points for January-February with a 2-hour model output). Statistically insignificant increments at the 95% significance level are marked with shading. In Fig. 4 shading indicates statistically insignificant data on either temperature or RMC.

245  
246  
247  
248  
249

For a more detailed analysis of the PW effects on atmospheric circulation, the time series of zonal-mean temperature and zonal wind variations due to the considered PW effects were observed – Fig. 4 and 5, respectively. Latitudes and heights corresponding to the maxima of the PW amplitudes were selected: the equator, 100 km is for the UFKW; 5-day wave is considered at 50° S and 105 km; 7-, 10- and 16-day waves: 50° N and 55 km; 4-day wave: 45° S and 105 km.



250

251

252

**Figure 5. Time series of zonal-mean zonal wind variations due to the inclusion of tropospheric sources of various PW in the regions of their maximum amplitudes in the MUAM.**

253

254

255

256

257

258

259

260

In all cases, especially for the zonal wind (Fig. 5), the wave structure of increments with a period corresponding to the period of the considered PW is observed. In particular, wind changes, which significantly exceed the averaged data for January and February (presented in Fig. 3) can be seen in this figure. Specifically, the inclusion of 16-day wave and the UFKW can cause the wind speed changes up to 4 m/s, and up to 5 m/s, respectively. PWs with zonal number 2 (4- and 7-day) make much smaller changes to the zonal flow, while, the weakening of the zonal flow is accompanied by the increase of these waves, as well as the 5-day wave and the UFKW by the end of February. Temperature variations in Fig. 4 have a more complex structure since temperature variations are affected not only by pressure fluctuations, but also by meridional circulation fluctuations.

261

## 5 Conclusion and summary

262

263

264

265

266

267

268

269

A number of model simulation have been carried out for January-February, using a 3-dimensional nonlinear mechanistic numerical model of the general circulation of the middle and upper atmosphere MUAM, to estimate the sensitivity of the atmosphere dynamic and thermal regime to the various planetary waves impact. The MUAM model allows to include selectively sources of various PW modes, which gives the opportunity to deeper study the contribution of each PW to the atmospheric circulation structure. Moreover, for a more detailed diagnostics of the PW effect on the mean flow, the transformed Eulerian mean approach was used, implying the calculation of the residual mean meridional circulation, which is a superposition of eddy and advective mean transport.

The amplitudes of the simulated PWs are consistent with the ground-based, satellite observations data, as well as with

270 the reanalysis and assimilation of meteorological data. The obtained increments of hydrometeorological parameters are  
271 maximal, as a rule, in the regions of maximum amplitudes of the considered PWs. In particular, the inclusion of 5-day PW and  
272 an UFKW can transform the components of the residual meridional circulation up to 6% each forming a significant contribution  
273 to the atmospheric circulation. The impact of the 16-day wave on the circulation is comparable in value with 5-day PW and  
274 UFKW, however it has a different structure. Changes in circulation components occur in the high-latitude stratosphere and may  
275 reach up to 6%. In turn, all the above mentioned changes in the meridional circulation, especially its vertical component, as  
276 well as variations of wave activity fluxes, can cause variations in the background temperature of more than 1 K. At the same  
277 time, at certain moments, this effect is much stronger. In addition, the waves can be superimposed on one another, and their  
278 effect can be summarized. I.e., the cumulative effect of the considered waves can significantly increase at certain moments of  
279 time.

280 The effect of 16-day PW generation by an internal atmospheric source in the southern lower thermosphere,  
281 independent of the tropospheric PW sources specified in the model, was found. Most probably, the point is that 4-day PW with  
282 a wave number 2 interacts nonlinearly with a 5-day PW with a wave number 1 causing a secondary wave excitation. Such  
283 mechanism is described, e.g., by Pogoreltsev (2001): when two waves having frequencies  $\omega$  and zonal numbers  $m$  interact, a  
284 new (secondary) wave arises, in which the frequency and wave number are the sum or difference of the corresponding values  
285 of the primary waves. Hence, the direct effect of the PWs can be enhanced due to their nonlinear interactions. Finally, this  
286 causes deceleration of the mean flow, creating better conditions for the SSW onset (e.g., Pogoreltsev et al., 2014). However,  
287 additional calculations are required to confirm this theory.

288 In addition, it should also be noted that for proper modelling of large-scale atmospheric dynamics, all models of the  
289 general atmospheric circulation should be tested for the ability to reproduce the global resonant properties of the atmosphere  
290 (the so-called atmospheric normal modes). This possibility has been repeatedly described in MUAM (e.g., Pogoreltsev, 2007,  
291 Koval et al., 2021), which underlines the reliability of the results obtained.

292  
293 **Author Contributions:** All authors have made valuable contributions in writing and editing of the manuscript, data  
294 analysis and visualization of the results. A.V.K.: conceptualization, RMC calculation, writing the final version of the  
295 manuscript; T.O.N., M.A.M.: numerical modelling; T.S.E. and K.A.D.: statistical processing; G.N.M.: consulting, English  
296 editing; E.V.R.: consulting, reanalysis data processing. All authors have read and agreed to the published version of the  
297 manuscript.

298 **Acknowledgements.** Calculations and interpretation of the residual mean circulation, statistical analysis are  
299 supported by the Russian Science Foundation (grant # 20-77-10006). MUAM adjustment, performing numerical simulations  
300 of the atmospheric global circulation and calculation of PW structures are supported by the Ministry of Science and Higher  
301 Education of the Russian Federation (agreement 075-15-2021-583). All figures in this study are made using Grid Analysis and  
302 Display System (GrADS), which is a free software developed thanks to the NASA Advanced Information Systems Research  
303 Program.

304 **Availability of data and materials.** According to the statement 1296 of the Civil Code of the Russian Federation, all  
305 rights on the MUAM code belong to the Russian State Hydrometeorological University (RSHU). To get access to the codes  
306 and for their usage a reader should get a permission from the RSHU Rector at the address 79, Voronezhskaya street, St.  
307 Petersburg, Russia, 192007, phone: 007 (812) 372-50-92. The authors will assist in getting such permission. All data sets  
308 presented in the paper can be obtained from the corresponding author (Andrey Koval, a.v.koval@spbu.ru) upon request.

309 **Competing interests.** The authors declare that they have no competing interests.

## 310 **References:**

311 Andrews, D. G. and McIntyre, M. E.: Planetary waves in horizontal and vertical shear: The generalized Eliassen-Palm relation  
312 and the mean zonal acceleration, *J. Atmos. Sci.*, 33, 2031–2048, [https://doi.org/10.1175/1520-](https://doi.org/10.1175/1520-0469(1976)033<2031:PWIHAV>2.0.CO;2)  
313 0469(1976)033<2031:PWIHAV>2.0.CO;2, 1976.

314 Butchart, N.: The Brewer-Dobson circulation, *Rev. Geophys.*, 52, 157—184, <https://doi.org/10.1002/2013RG000448>, 2014.

315 Chang, L. C., Yue, L., Wang, W., Wu, Q., and Meier, R. R.: Quasi two day wave-related variability in the background dynamics  
316 and composition of the mesosphere/thermosphere and the ionosphere, *Journal of Geophysical Research: Space Physics.*, 119,  
317 6, 4786–4804, 2014.

318 Charney, J. G. and Drazin, P. G.: Propagation of planetary-scale disturbances from the lower into the upper atmosphere, *J.*  
319 *Geophys. Res.*, 66, 83–109, 1961.

320 Clark, R., Burrage, M., Franke, S., Manson, A., Meek, C., Mitchell, N., and Muller, H.: Observations of 7-d planetary waves  
321 with MLT radars and the UARS-HRDI instrument, *Journal of Atmospheric and Solar-Terrestrial Physics*, 64 ,8/11, 1217–  
322 1228, 2002.

323 Day, K. A., Hibbins, R. E., and Mitchell, N. J.: Aura MLS observations of the westward-propagating 16-day planetary wave  
324 in the stratosphere, mesosphere and lower thermosphere, *Atmos. Chem. Phys.*, 11, 4149–4161, [https://doi.org/10.5194/acp-](https://doi.org/10.5194/acp-11-4149-2011)  
325 11-4149-2011, 2011.

326 Drob, D. P., Emmert, J. T., Meriwether, J. W., Makela, J. J., Doornbos, E., Conde, M., Hernandez, G., Noto, G., Zawdie, K.  
327 A., McDonald, S. E., Huba, J. D., and Klenzing, J. H.: An update to the Horizontal Wind Model (HWM): The quiet time  
328 thermosphere, *Earth and Space Science*, 2, 301–319, <https://doi.org/10.1002/2014EA000089>, 2015.

329 Eliassen A. and Palm E.: On the transfer of energy in stationary mountain waves // *Geophys. Norv.*, 22, 1—23, 1961.

330 Emmert, J. T., Drob, D. P., Picone, J. M., Siskind, D. E., Jones, M. Jr., Mlynczak, M. G., et al.: NRLMSIS 2.0: A whole-  
331 atmosphere empirical model of temperature and neutral species densities, *Earth and Space Science*, 7, e2020EA001321,  
332 <https://doi.org/10.1029/2020EA001321>, 2020.

333 Ermakova T. S., Aniskina, O. G., Statnaya, I. A., Motsakov, M. A., and Pogoreltsev A. I.: Simulation of the ENSO influence  
334 on the extra-tropical middle atmosphere, *Earth, Planets and Space*. 71, 8, <https://doi.org/10.1186/s40623-019-0987-9>, 2019.

335 Forbes, J. M. and Zhang, X.: The quasi-6 day wave and its interactions with solar tides, *Journal of Geophysical Research:*  
336 *Space Physics*, 122, 4764–4776, <https://doi.org/10.1002/2017JA023954>, 2017.

337 Forbes, J. M., Zhang, X., and Maute, A.: Planetary wave (PW) generation in the thermosphere driven by the PW-modulated  
338 tidal spectrum, *Journal of Geophysical Research: Space Physics*, 125, e2019JA027704,  
339 <https://doi.org/10.1029/2019JA027704>, 2020.

340 Forbes, J. M., Zhang, X., Maute, A., and Hagan, M. E.: Zonally symmetric oscillations of the thermosphere at planetary wave  
341 periods, *Journal of Geophysical Research: Space Physics*, 123, 4110–4128, <https://doi.org/10.1002/2018JA025258>, 2018.

342 Gavrilov, N. M., Koval, A. V., Pogoreltsev, A. I., and Savenkova, E. N.: Simulating planetary wave propagation to the upper  
343 atmosphere during stratospheric warming events at different mountain wave scenarios, *Advances in Space Research*. 61, 7,  
344 1819–1836, 2018. DOI: 10.1016/j.asr.2017.08.022

345 Gelaro, R., McCarty, W., Suárez, Max J., Todling, R., Molod, A., Takacs, L., Randles, C., Darmenov, A., Bosilovich, M. G.,  
346 Reichle, R., Wargan, K., Coy, L., Cullather, R., Draper, C. , Akella, S., Buchard, V., Conaty, A. , da Silva, A., Wei Gu, Gi-  
347 Kong Kim, Koster, R., Lucchesi, R., Merkova, D., Nielsen, J. E., Partyka, G., Pawson, S., Putman, W., Rienecker, M.,  
348 Schubert, S. D., Sienkiewicz, M. and Zhao, B. The Modern-Era Retrospective Analysis for Research and Applications, Version  
349 2 (MERRA-2), *J. Clim.*, Volume 30, 13, 5419–5454, <https://doi.org/10.1175/JCLI-D-16-0758.1>, 2017.

350 Haynes, P. H., McIntyre, M. E., Shepherd, T. G., Marks, C. J., and Shine, K. P. On the “downward control” of extratropical  
351 diabatic circulations by eddy-induced mean zonal forces, *J. Atmos. Sci.* 48, 4, 651–678, 1991.

352 He, M., Chau, J. L., Forbes, J. M., Thorsen, D., Li, G., Siddiqui, T. A., et al.: Quasi-10-day wave and semidiurnal tide nonlinear  
353 interactions during the Southern Hemispheric SSW 2019 observed in the Northern Hemispheric mesosphere, *Geophysical*  
354 *Research Letters*, 47, e2020GL091453, <https://doi.org/10.1029/2020GL091453>, 2020.

355 Holton, J. R.: The dynamic meteorology of the stratosphere and mesosphere, *Meteorol. Monogr.* 15, 37, 218 p., 1975.

356 Holton, J. R., Haynes, P. H., McIntyre, M. E., Douglas, A. R., Rood, R. B., and Pfister, L.: Stratosphere-troposphere exchange,  
357 *Rev. Geophys.* 33, 403–439, 1995.

358 Holton, J. R. and Tan, H.: The influence of the equatorial quasibiennial oscillation on the global circulation at 50 mb, *J. Atmos.*  
359 *Sci.* 37, 2200–2208, 1980.

360 Huang, Y., Zhang, S., Li, C., Li, H., Huang, K., and Huang, C.: Annual and interannual variations in global 6.5 DWS from 20  
361 to 110 km during 2002–2016 observed by TIMED/SABER, *Journal of Geophysical Research: Space Physics*, 122, 8985–9002,  
362 <https://doi.org/10.1002/2017JA023886>, 2017.

363 Jacobi, Ch., Fröhlich, K., and Portnyagin, Y. Semi-empirical model of middle atmosphere wind from the ground to the lower  
364 thermosphere, *Adv. Space Res.* 43, 239–246, 2009.

365 Jiang, G.-y., Xu, J., Xiong, J., Ma, R., Ning, B., Murayama, Y., et al.: A case study of the mesospheric 6.5-day wave observed  
366 by radar systems, *Journal of Geophysical Research*, 113, D16111, <https://doi.org/10.1029/2008JD009907>, 2008.



367 Koval, A. V., Gavrilov, N. M., Pogoreltsev, A. I., and Kandieva, K. K.: Dynamical impacts of stratospheric QBO on the global  
368 circulation up to the lower thermosphere, *Journal of Geophysical Research: Atmospheres*, 127, e2021JD036095, 2022a.  
369 <https://doi.org/10.1029/2021JD036095>.

370 Koval, A.V., Gavrilov, N.M., Kandieva, K.K. Ermakova, T.S., Didenko, K.A. Numerical simulation of stratospheric QBO  
371 impact on the planetary waves up to the thermosphere. *Scientific Reports*, 12, 21701, 2022b. DOI: 10.1038/s41598-022-26311-  
372 x

373 Koval, A. V., Gavrilov, N. M., Pogoreltsev, A. I., and Shevchuk, N. O.: Influence of solar activity on penetration of traveling  
374 planetary-scale waves from the troposphere into the thermosphere, *Journal of Geophysical Research: Space Physics*, 123, 8,  
375 6888–6903, <https://doi.org/10.1029/2018JA025680>, 2018a.

376 Koval, A. V., Gavrilov, N. M., Pogoreltsev, A. I., and Savenkova, E. N.: Comparisons of planetary wave propagation to the  
377 upper atmosphere during stratospheric warming events at different QBO phases, *Journal of Atmospheric and Solar-Terrestrial*  
378 *Physics*, 171, 201-209, <https://doi.org/10.1016/j.jastp.2017.04.013>, 2018b.

379 Liu, H. L., Talaat, E. R., Roble, R. G., Lieberman, R. S., Riggins D. M., and Yee, J. H.: The 6.5-day wave and its seasonal  
380 variability in the middle and upper atmosphere, *Journal of Geophysical Research-Atmospheres*, 109, D21,  
381 <https://doi.org/10.1029/2004jd004795>, 2004.

382 Longuet-Higgins, M. S.: The eigenfunctions of Laplace's tidal equation over a sphere. *Philos. T. R. Soc. Lond.* 262: 511–607,  
383 1968.

384 Matsuno, T. Vertical propagation of stationary planetary waves in the winter Northern Hemisphere. *J. Atmos. Sci.* 27(6),  
385 871–883, 1970.

386 Medvedeva, I. V., Semenov, A. I., Pogoreltsev, A. I., and Tatarnikov, A. V.: Influence of sudden stratospheric warming on the  
387 mesosphere/lower thermosphere from the hydroxyl emission observations and numerical simulations, *Journal of Atmospheric*  
388 *and Solar-Terrestrial Physics*, 187, 22–32, <https://doi.org/10.1016/j.jastp.2019.02.005>, 2019.

389 Merzlyakov, E., Solovjova, T., and Yudakov, A.: The interannual variability of a 5–7 day wave in the middle atmosphere in  
390 autumn from era product data, aura MLS data, and meteor wind data, *Journal of Atmospheric and Solar-Terrestrial Physics*,  
391 102, 281–289, 2013.

392 Nath, D., Chen, W., Zelin, C., Pogoreltsev, A. I., and Wei, K. Dynamics of 2013 Sudden Stratospheric Warming event and its  
393 impact on cold weather over Eurasia: Role of planetary wave reflection, *Sci. Rep.* 6, 24174, <https://doi.org/10.1038/srep24174>,  
394 2016.

395 Newman, P. A., Oman, L. D., Douglass, A. R., Fleming, E. L., Frith, S. M., Hurwitz, M. M., Kawa, S. R., Jackman, C. H.,  
396 Krotkov, N. A., Nash, E. R., Nielsen, J. E., Pawson, S., Stolarski, R. S., and Velders, G. J. M.: What would have happened to  
397 the ozone layer if chlorofluorocarbons (CFCs) had not been regulated? *Atmos. Chem. Phys.*, 9, 2113–2128,  
398 <https://doi.org/10.5194/acp-9-2113-2009>, 2009.

399 Pancheva, D., Mukhtarov, P., Andonov, B., and Forbes, J. M.: Global distribution and climatological features of the 5-6-day  
400 planetary waves seen in the SABER/TIMED temperatures (2002-2007). *J. Atmos. Solar-Terr. Phys*, 72, 1, 26–37, 2010.

401 Pancheva, D., Mukhtarov, P., Andonov, B., Mitchell, N. J., and Forbes, J. M. Planetary waves observed by TIMED/SABER  
402 in coupling the stratosphere- mesosphere-lower thermosphere during the winter of 2003/2004: part 2—altitude and latitude  
403 planetary wave structure, *J. Atmos. Solar-Terr. Phys.* 71, 1, 75–87, <https://doi.org/10.1016/j.jastp.2008.09.027>, 2009.

404 Pancheva, D., Mukhtarov, P., Mitchell, N. J., Merzlyakov, E., Smith, A. K., Andonov, B., Singer, W., Hocking, W., Meek, C.,  
405 Manson, A., and Murayama, Y. Planetary waves in coupling the stratosphere and mesosphere during the major stratospheric  
406 warming in 2003/2004, *J. Geophys. Res.* 113, D12, D12105, <https://doi.org/10.1029/2007JD009011>, 2008.

407 Pancheva, D., Mukhtarov, P., and Siskind, D. E.: The quasi-6-day waves in NOGAPS-ALPHA forecast model and their  
408 climatology in MLS/Aura measurements (2005–2014), *Journal of Atmospheric and Solar-Terrestrial Physics*, 181, 19–37,  
409 2018.

410 Pedatella, N. M. and Forbes, J. M.: Modulation of the equatorial F-region by the quasi-16-day planetary wave, *Geophys. Res.*  
411 *Letts.*, 36, L09105, <https://doi.org/10.1029/2009GL037809>, 2009.

412 Pogoreltsev, A. I. (2007). Generation of normal atmospheric modes by stratospheric vacillations. *Izvestiya Atmos. Ocean.*  
413 *Phys.* 43(4), 423–435.

414 Pogoreltsev, A. I. Numerical simulation of secondary planetary waves arising from the nonlinear interaction of the normal  
415 atmospheric modes. *Phys. Chem. Earth (Part C)*. 26(6), 395–403 (2001).

416 Pogoreltsev, A. I.: Simulation of planetary waves and their influence on the zonally averaged circulation in the middle  
417 atmosphere, *Earth, Planets Space*. 51, 7/8, 773–784, 1999.

418 Pogoreltsev, A.I., Vlasov, A.A., Froehlich, K., and Jacobi, Ch.: Planetary waves in coupling the lower and upper atmosphere,  
419 *J. Atmos. Solar-Terr. Phys.* 69, 2083–2101, <https://doi.org/10.1016/j.jastp.2007.05.014>, 2007.

420 Qin, Y., Gu, S.-Y., and Dou, X.: A new mechanism for the generation of quasi-6-day and quasi-10-day waves during the 2019  
421 Antarctic sudden stratospheric warming, *Journal of Geophysical Research: Atmospheres*, 126, e2021JD035568,  
422 <https://doi.org/10.1029/2021JD035568>, 2021.

423 Pogoreltsev, A. I., Savenkova, E. N., Pertsev, N. N. Sudden stratopheric warmings: the role of normal atmospheric modes.  
424 *Geomagnetism and Aeronomy* 54(2), 1–15, 2014. doi 10.1134/S0016793214020169

425 Sassi, F., Garcia, R., and Hoppel, K.: Large-scale Rossby normal modes during some recent Northern Hemisphere winters,  
426 *Journal of the Atmospheric Sciences*, 69, 3, 820–839, 2012.

427 Schoeberl, M.: Stratospheric warmings – observations and theory, *Rev. Geophys.* 16, 521–538.  
428 <https://doi.org/10.1029/RG016i004p00521>, 1978.

429 Shevchuk N. O., Ortikov M. Yu., Pogoreltsev, A. I. Modeling of atmospheric tides with account of diurnal variations of  
430 ionospheric conductivity. *Russian Journal of Physical Chemistry B*. V. 12(3), 576–589, 2018. DOI:  
431 10.1134/S199079311803017X.

432 Suvorova, E. V., Pogoreltsev, A. I. Modeling of nonmigrating tides in the middle atmosphere. *Geomagnetizm and Aeronomy*.  
433 51(1), 105-115, 2011. DOI: 10.1134/S0016793210061039

434 Swarztrauber, P. N. and Kasahara, A.:The vector harmonic analysis of Laplace's tidal equations, SIAM J. Sci. Stat. Comp. 6,  
435 464–491, 1985.

436 Wang, J. C., Chang, L. C., Yue, J., Wang, W., and Siskind, D. E.: The quasi 2 day wave response in TIME-GCM nudged with  
437 NOGAPS-ALPHA, Journal of Geophysical Research: Space Physics, 122, 5, 5709–5732, 2017.

438 Yamazaki, Y., Matthias, V., and Miyoshi, Y.: Quasi-4-day wave: Atmospheric manifestation of the first symmetric Rossby  
439 normal mode of zonal wavenumber 2, Journal of Geophysical Research: Atmospheres, 126, e2021JD034855,  
440 <https://doi.org/10.1029/2021JD034855>, 2021.

441